# EFFECT OF Hg ON $CO_2$ CAPTURE BY SOLID SORBENTS IN THE PRESENCE OF ACID GASES

N. Fernández-Miranda[a], S. García[b], M.A. Lopez-Anton[a]*, M.R. Martínez-Tarazona[a], E.S. Sanz-Pérez[c], M.M. Maroto-Valer[b]

[a]Instituto Nacional del Carbón (CSIC), Francisco Pintado Fe, 26, 33011, Oviedo, Spain

[b]Centre for Innovation in Carbon Capture and Storage (CICCS), School of Engineering & Physical Sciences, Heriot-Watt University, Edinburgh, EH14 4AS, United Kingdom

[c]Department of Energy and Chemical Technology, ESCET. Universidad Rey Juan Carlos, C/ Tulipán s/n, 28933 Móstoles, Madrid, Spain

*Corresponding author:

Phone: +34 985 119090
Fax: +34 985 297662
Email: marian@incar.csic.es

**Abstract**

Carbon dioxide Capture and Storage (CCS) is the main technology to mitigate $CO_2$ emissions in the energy sector, being reversibly adsorption of $CO_2$ on solid sorbents one of the most promising processes to be operated in post-combustion technology. Given the current state of development a number of problems still need to be addressed before solid sorbents can be employed for $CO_2$ capture. One of these problems is the effect that some impurities in the flue gas have on the behavior of the sorbents. The aim of this work is to identify and evaluate the role of mercury species in flue gas containing acid gases on the performance of sorbents employed for $CO_2$ capture. The influence of mercury on $CO_2$ retention capacity was assessed using three commercial activated carbons (NORIT GCN, AIRPEL 1DS-1 and AIRPEL ULTRA DS5) and two mesostructured silica sorbents containing amino groups (SBA-PEI and SBA-TEPA). When $Hg^0$ was incorporated into the gas stream, the behaviour of the sorbents was modified. In general, the $CO_2$ adsorption capacity decreased in the presence of $Hg^0$ suggesting competition by both compounds for the same active sites. The strongest effect of $Hg^0$ on $CO_2$ adsorption was observed in the activated carbon with the highest micropore volume.

**Keywords**: mercury; carbon dioxide; adsorption; coal combustion

## 1. Introduction

Global warming and climate change have motivated a great effort on research activities toward developing efficient processes to mitigate $CO_2$ emissions. Among the possibilities, Carbon Capture and Storage (CCS) is the main technology used in the energy sector. This process consists of capturing and compressing $CO_2$, which is then transported and deposited safely. Depending on where and how the $CO_2$ capture process is carried out, this step is classified as (i) post-combustion, (ii) pre-combustion and (iii) oxy-fuel combustion technologies. Among them, post-combustion is a suitable option for retrofitting existing power plants and several post-combustion routes could be used: wet absorption, dry adsorption, membrane-based technologies and cryogenics. Although each one of these have advantages and disadvantages, the main drawback of most of them is that they are expensive and energy intensive [1]. Absorption is the most mature and high efficient $CO_2$ separation process but issues related to environmental impact of this process still need to be controlled [2]. Currently, there is a growing interest in adsorption processes using solid sorbents capable of reversibly capturing $CO_2$ because this technology shows promise to decrease the associated costs. In this sense, the use of solid adsorbents reduces the energy needed for the regeneration step, possess greater capacity and selectivity, and can be more easily handled compared to other post-combustion $CO_2$ capture processes [3].

The success of novel adsorption technologies is dependent on the development of new materials with high $CO_2$ adsorption capacity and selectivity, durability and relatively fast kinetics of adsorption and desorption [4]. Typical sorbents include molecular sieves, activated carbons, zeolites, calcium oxides, hydrotalcites and lithium zirconates [2,5].

Carbon-based materials are considered as one of the most promising adsorbents [6] due to their low cost, high surface area, high amenability to pore structure modification and surface functionalization, and relative easiness for regeneration. However, the $CO_2$ adsorption on carbon materials is physical and weak which makes these adsorbents sensitive to temperature and relatively poor in selectivity [4,8].

Adsorption of $CO_2$ using amine-functionalized sorbents involves chemical reactions and, therefore, it is necessary to know how the nature of the amine influences the rate of adsorption and kinetics in terms of amine efficiency, defined as the number of $CO_2$ molecules adsorbed for each nitrogen atom present in the amine-containing solid [4,5,9,10].

Regardless of the kind of adsorption process (physisorption or chemisorption), solid sorbents have limitations and challenges to be solved before they can be employed commercially [4]. This work is focused on the effect of mercury species present in the flue gas on sorbent performance. Flue gas from a coal-fired thermal power facility typically contains 70-80% $N_2$, 11-15% $CO_2$, 5-12% $H_2O$, 3-6% $O_2$, 200-4000 ppm $SO_x$, 200-800 ppm $NO_x$, 50-100 ppm CO and 25–50 ppm HCl, with traces of mercury species and other volatile elements. It has been observed that $SO_x$, $NO_x$ [4,11,12] and water vapour [13], might exhibit a detrimental effect on physical $CO_2$ sorption. However, to the best of the authors' knowledge, the effect of mercury species on $CO_2$ capture in solid adsorbent has not been considered so far.

Coal combustion is the largest single anthropogenic source of mercury to air [14]. However, mercury concentration and speciation in flue gas significantly differ as a consequence of the characteristics of the coal and the power plant configuration. Differences in mercury composition are mainly associated with the performance of DeNOx plants (mainly SCR), particle control devices and flue gas desulfurization

systems. Although concentration of mercury in the combustion gases up to 70 $\mu g/m^3$ have been reported, in general, mercury content in coal combustion gases is below 10 $\mu g/m^3$ [15], bound to particulate matter ($Hg_p$) or remaining in the vapor state as oxidized ($Hg^{2+}$) or elemental ($Hg^0$) mercury [16,17].

Thus, the aim of this study is to evaluate the effect of gaseous mercury species on the sorbent performance for $CO_2$ capture via physical of chemical adsorption, focusing on potential co-adsorption of $CO_2$ and Hg species on specific solid sorbents. The solids evaluated were three commercial activated carbons and two mesostructured silica sorbents where different amino groups had been incorporated.

## 2. Experimental part.

### 2.1. Sorbents for $CO_2$ capture.

The sorbents studied were three commercial activated carbons NORIT-CGN, AIRPEL 1DS-1 and AIRPEL DS5 named AC-1, AC-2 and AC-3, respectively, and two mesostructured silica sorbents incorporating amino groups, SBA-PEI and SBA-TEPA. The activated carbon AC-1 has been produced from coconut shell by means of a steam physical activation, and AC-2 and AC-3 are two extruded activated carbons from anthracite coals with enhanced adsorption capacity for $H_2S$, $SO_2$, mercaptans and acid compounds, especially developed for air purification applications.

The amino-functionalized sorbents were obtained by impregnation of calcined SBA-15 [18,19] with two organic polymers: branched polyethyleneimine (PEI, average molecular weight 800, Sigma-Aldrich) and tetraethylenepentamine (TEPA, Sigma-Aldrich) following the procedure described by Xu et al. [20,21] and resulting in a final product with 30% weight of organic component (SBA-PEI and SBA-TEPA).

2.2. Characterization of sorbents.

Textural properties of activated carbons were determined from $CO_2$ adsorption isotherms at 298 K in a Quantachrome Analyser. The micropore volume, the pore diameter and the adsorption energy were calculated by means of the Dubinin-Radushkevich (DR) equation. In the case of activated carbon samples, the DR equation provides valuable information because it allows the calculation of the micropore volume using the low-pressure zone of the adsorption isotherm. The DR equation relates the volume of the adsorbed gas to the relative pressure (P / P °), through the micropore volume parameter and the pore size of the solid.

Surface chemical characterization was performed by temperature-programmed desorption (TPD) using an Autochem II Analyzer coupled to an Omnistar$^{TM}$ mass detector in an argon atmosphere at 10ºC/min.

Textural properties of SBA-PEI and SBA-TEPA sorbents were determined from nitrogen adsorption-desorption isotherms at 77 K in a Micromeritics Tristar 3000. Surface area was calculated following the Brunauer-Emmett-Teller (BET) equation and the pore size distribution was obtained by means of the B.J.H. model assuming cylindrical geometry of the pores [22]. The analysis of nitrogen was carried out in a Thermo Flash EA 1112 analyzer equipped with a MAS 200R autosampler [19].

The microstructure and morphology of the sorbents were characterized by Scanning Electron Microscopy (SEM) using a Philips XL30 ESEM and a Quanta FEG 650 microscopes, equipped with energy dispersive analytical systems (EDAS). Fourier transform-infrared spectra (FT-IR) were recorded for pelletized samples diluted in KBr. A Varian 3100 and a Nicolet 8700 device were used to analyse the silica and activated carbon sorbents, respectively. Sample stability was tested by thermogravimetric analysis

in a Mettler-Toledo TGA/DSC 1 instrument. The samples were heated up to 700ºC at a heating rate of 5ºC/min in a 100 mL/min flow of compressed air.

2.3. Experimental devices.

2.3.1 $CO_2$ adsorption tests.

$CO_2$ adsorption capacity of the sorbents was evaluated under different flue gas compositions in cyclic adsorption-desorption experiments. After a degasification step for 2 hours at 110 ºC to remove moisture and adsorbed gases, 120 mL·min$^{-1}$ of $N_2$ was allowed to flow through the system at atmospheric pressure for 10 minutes as a pre-conditioning phase. Afterwards, an adsorption step was carried out in which a constant inlet flowrate of 120 mL·min$^{-1}$ of the diverse gas mixtures were fed through a fixed reactor (length: 500 mm, diameter: 25 mm) for ten minutes at room temperature and atmospheric pressure (Figure 1). This time was long enough to reach the saturation of the sorbents. The sorbent bed was prepared by mixing 0.25 g of sorbent with 0.75 g of sand in order to avoid an excess of pressure in the system. A mass spectrometer Pfeiffer Vacuum OmniStar QMG220 was used for determining the $CO_2$ adsorbed. Table 1 shows the composition of the atmospheres used in the work: $N_2$+$CO_2$, $N_2$+$CO_2$+Hg and the designed as CA (complete atmosphere). The $CO_2$ adsorbed was desorbed by switching the flowrate to 120 mL·min$^{-1}$ of $N_2$ for five minutes. All sorbents tested were subjected to eight adsorption-desorption cycles by which the $CO_2$ adsorption capacity was assessed under the different flue gas compositions by mass spectroscopy. A blank analysis was used to calculate the void volume due to the tubbing and the interparticle space of the sorbents.

2.3.2 $CO_2$ /Hg adsorption tests.

The $CO_2$ adsorption capacity of the sorbents in the presence of $Hg^0$ in the flue gas was assessed in the laboratory scale device described in Figure 1 including a generation unit for elemental mercury and a continuous mercury analyser VM-3000 that monitored $Hg^0$ in gas phase.

A calibrated permeation tube VICI Metronic was placed inside a glass "U" tube immersed in a water bath at 40ºC to obtain 500 $\mu g \cdot m^{-3}$ $Hg^0$ in the gas phase. The carrier gas used consisted of $N_2$ that, subsequently, was mixed with different proportions of $CO_2$, $SO_2$, $O_2$ and HCl (Table 1).

The possible oxidized mercury ($Hg^{2+}$), which may have been formed by homogeneous or heterogeneous oxidation, was evaluated by circulating the gas through an ion exchange resin DOWEX 1x8, suitable for the selective extraction and capture of $Hg^{2+}$ species [23]. The resin was conditioned before use with a solution of HCl:$H_2O$ [1:1] at 90ºC for 30 min and then filtered and dried and it was placed prior the mass spectrometer and immediately after the fixed bed reactor (Figure 1). The resin was previously tested to prove that $CO_2$ is not captured in this material. The mercury retained in the sorbents and in the resin after the experiments was determined using a LECO Mercury Analyser, AMA 254.

## 3. Results and discussion.

### 3.1. Characterization of the sorbents.

The porous textural characteristics of AC-1, AC-2 and AC-3 were compared using adsorption isotherms of $CO_2$ at 298 K (Figure 2) [24]. As it can be observed in Table 2, fitting the Dubinin–Radushkevich equation to the isotherms (affinity coefficient $\beta = 0.35$ and $CO_2$ density $\rho = 1.044$ g·cm$^{-3}$) yielded micropore volumes ($V_{DR}$)

of 0.28 $cm^3 \cdot g^{-1}$ (AC-1), 0.17 $cm^3 \cdot g^{-1}$ (AC-2) and 0.19 $cm^3 \cdot g^{-1}$ (AC-3) and micropore diameters ($W_{DR}$) of 0.88 nm, 0.85 nm and 0.88 nm for AC-1, AC-2 and AC-3, respectively ($R^2$= 0.9989). The $CO_2$ adsorption energy ($E_{DR}$) presented similar values for AC-1 and AC-3 (10.26 and 10.32 $kJ \cdot mol^{-1}$), being slightly lower than that obtained with AC-2 (10.70 $kJ \cdot mol^{-1}$), which corroborates the inversely proportional relationship between the adsorption energy and the micropore diameter.

A higher macroporosity in AC-1 was observed in the micrographs obtained by SEM (see Supplementary Figure S1). Apart from their morphology, analysis by SEM/EDAS revealed a higher amount of mineral matter in the AC-2 and AC-3 activated carbons. This was confirmed by the characteristic band of mineral matter at 750 $cm^{-1}$ identified by FT-IR (see Supplementary Figure S2).

The most significant characteristics of the amino-functionalized SBA-15 silica sorbents, already reported in a previous work [19], are summarized in Table 3. $N_2$ adsorption-desorption isotherms showed the coexistence of micro and mesoporous. The surface area was 153 $m^2 \cdot g^{-1}$ for SBA-PEI and 220 $m^2 \cdot g^{-1}$ for SBA-TEPA ($R^2$= 0.9999), with a pore diameter of 5.8 nm and 9.0 nm for SBA-PEI and SBA-TEPA, respectively, and a pore volume of 0.27 and 0.45 $cm^3 \cdot g^{-1}$. Nitrogen content was greater in the SBA-TEPA adsorbent (8.8 wt %) than in SBA-PEI (5.8 wt %), due to its higher nitrogen content per molecule.

Analysis of the amine sorbents by SEM (see Supplementary Figure S3) revealed a typical SBA-15 morphology. Hydrocarbon chains were not visible as their density is lower than that of the bulk silica. The impregnated samples (SBA-PEI and SBA-TEPA) showed a higher aggregation than raw SBA-15. However, no differences in the chainlike structure of SBA-15 after impregnation were observed.

As expected, silanol groups on the silica surface and adsorbed water were responsible for three prominent absorption bands observed by FT-IR at 3700-3200 $cm^{-1}$ (O-H and SiO-H, stretching vibrations), 1631 $cm^{-1}$ (O-H bending in physisorbed water) and 962 $cm^{-1}$ (SiO-H bending) (see Supplementary Figure S4). The presence of 30 % PEI or TEPA in the impregnated adsorbents yielded new bands related to hydrocarbon chains and amino groups.

Thermogravimetric analyses of the silica sorbents showed that SBA-PEI and SBA-TEPA are stable up to 160 ºC in air (see Supplementary Figure S5). Although slow reactions might take place even at mild temperatures like 110ºC, it must be taken into consideration that these sorbents are intended to be used at the end of the cycle of coal combustion plants where the temperature is around 40-60ºC. In the case of activated carbon samples they are stable up to 300ºC (see Supplementary Figure S6).

3.2. $CO_2$ adsorption capacity.

With the aim to assess the influence of mercury in the $CO_2$ adsorption, the sorbents were firstly evaluated in the absence of Hg. The $CO_2$ adsorption capacity at equilibrium of the activated carbons was obtained from the results of the pure $CO_2$ isotherms (Figure 2), showing different behavior for each type of carbon sorbent. Anthracite-coal precursor carbons (AC-2 and AC-3) presented similar adsorption uptake, reaching 1.70 and 1.74 $mmol \cdot g^{-1}$ of $CO_2$ respectively, whereas AC-1 (coconut-shell precursor) showed adsorption values around 2.51 $mmol \cdot g^{-1}$. Previous works carried out with activated carbons in the same conditions of temperature and pressure as in this study have reported a wide range of $CO_2$ adsorption capacities (from 1.53 to 3.23 $mmol \cdot g^{-1}$) [24-28]. Activated carbons bind the $CO_2$ on their surface through physisorption processes, where the Van der Waals attraction between $CO_2$ and the adsorbent surface is the main cause of the selective adsorption of this compound [29].

Regarding the above mentioned, the highest $CO_2$ adsorption capacity of AC-1 could be a consequence of its higher narrow micropore volume (Table 2). In fact, $CO_2$ adsorption capacity under ambient conditions (25 ºC and 1 bar) is strongly correlated with the content of narrow carbon micropores [30-32] rather than with other parameters such as the specific surface area.

The $CO_2$ adsorption capacity in the amino-functionalized silica sorbents was evaluated in previous works [19]. In general, the silica sorbents showed a greater $CO_2$ adsorption than the activated carbons as the result of the dominant chemisorption processes between carbon dioxide and amino groups [33].

3.3. Effect of mercury in the $CO_2$ adsorption capacity.

After a concentration of 500 $\mu g \cdot m^3$ of $Hg^0$ was added to the inlet stream consisting of 15% $CO_2$ and 85% $N_2$, the $CO_2$ adsorption capacity decreased (Figure 3, Table 4) when compared to the same inlet stream with no $Hg^0$ content. The confidence limit of the results represented by the relative standard deviation is <15 %. This loss of the adsorption capacity was especially important in the case of AC-1 and SBA-PEI where drops of 65 and 32%, respectively, were recorded (Figure 3). In the case of the activated carbons AC-2 and AC-3 the reduction in the adsorption capacity was approximately 6-7%, whereas no differences were observed in SBA-TEPA (Figure 3). These results suggest that mercury affects the $CO_2$ adsorption capacity of the sorbents depending on their textural and chemical characteristics.

In order to clarify the effect of mercury on $CO_2$ adsorption, the retention of mercury in the sorbents was also evaluated in a similar experimental device as described in Figure 1 without $CO_2$ unit [35]. Figure 4 (A) shows the mercury adsorption curves in the atmosphere formed by 15% $CO_2$ + 85% $N_2$. The curves represent the Hg

concentration ratio ($C/C_o$) versus time where C is the Hg concentration registered after the sorbent bed and $C_o$ is the inlet Hg concentration. The concentration of Hg retained was calculated as the area between the curve and the background ($C/C_0$=1) at the time of 350 min. This time (350 min) was chosen as being a reasonable experimental duration of time for comparing the behaviour of the different sorbents under similar conditions. The mercury retention capacity was significantly higher in AC-1. Indeed, when AC-2 and AC-3 reached the mercury saturation ($C/C_0$=1) (at 350 min), near to 70% of mercury is being retained by AC-1 ($C/C_0$=0.3).The amount of mercury retained in SBA-PEI and SBA-TEPA was very low. The proportion of oxidized mercury ($Hg^{2+}$) registered at the reactor outlet during the experiments was negligible for all sorbents. Therefore, taking into account that homogeneous mercury oxidation did not occur in the atmospheres employed, if heterogeneous oxidation took place, all the oxidized mercury would have been retained.

By comparing the results above mentioned, a correlation between the $CO_2$ mass uptake and the mercury retained by each sorbent can be established. Concerning the activated carbons, those with higher mercury retention capacity exhibited a pronounceable drop in their $CO_2$ adsorption potential, being particularly noteworthy in the case of AC-1 (Table 4). This behavior suggests a competition of both species for the active sites on the surface.

Mercury interaction with sorbents may follow, in part, a physical adsorption mechanism [35,36]. If the relation between textural properties of these materials and mercury retention is examined, it is concluded that the sorbent with the highest microporous volume (AC-1) (Table 2) showed the highest mercury retention. These results are in agreement with those previously obtained [37,38] that have determined that the presence of micropores improves the mercury adsorptive capacity of activated

carbons as a consequence of the higher interaction potential inside micropores when compared to wider pores [39]. In fact, the mesoporous amino-functionalized silica sorbents hardly retain mercury (Table 4, Figure 4(A)). Additionally, mercury retention may be due not only to physical adsorption but it also may involve chemical adsorption [35,36,40,41]. TPD analyses (Figure 4 (B)) were carried out in the activated carbons to identify the type of surface oxygenated groups that may affect mercury retention. Previous works have suggested that oxygen functional groups, particularly lactones and carbonyls, may favour mercury adsorption whereas phenol groups would inhibit its adsorption [38,40-42]. From the release of CO, carbonyls and quinones (peaks centered at 850ºC) were only identified in AC-1, whereas the peaks centered at temperatures between 600 and 800ºC, corresponding to the decomposition of phenols and ethers, were identified in AC-2 and AC-3 (Figure 4 (B)). Therefore, the previous assumptions are in agreement with the results obtained in this study since the AC-1 sorbent, which retained the highest amount of mercury, showed TPD profiles representative of carbonyls and quinones groups; conversely, AC-2 and AC-3, for which the TPD profiles indicated the presence of phenol/ether groups, had a lower mercury retention capacity than AC-1. As can be observed in Figure 4(B) AC-2, which presented the highest amount of functional groups between 600-800ºC, exhibited the lowest mercury retention capacity (Table 4).

In the case of the amino-functionalized silica sorbents (Figure 3 (B), Table 4) it was observed a loss of the $CO_2$ adsorption capacity in presence of $Hg^0$ for SBA-PEI. Therefore, mercury again might be occupying part of the binding sites of $CO_2$ in PEI polymers, establishing a competitive interaction between both gases for the same adsorption sites.

3.4. Efficiency of the sorbents under post-combustion conditions.

Solid sorbents for $CO_2$ capture should be stable not only under the presence of trace elements, such as mercury, but also under an oxidizing environment, so they need to be tolerant to common flue gas contaminants, such as $SO_2$ and $NO_x$ [29]. Therefore, $CO_2$ capture capacity was also tested under other gases present during coal combustion (CA in Table 1). For all sorbents studied, the presence of acid-gas components leaded to a decrease in their $CO_2$ adsorption capacity (Figure 3). This loss of capacity was especially important for the sorbents SBA-TEPA and AC-1, which suffered a drop of 93%. The reduction in the $CO_2$ adsorption capacity for AC-2, AC-3 and SBA-PEI was 40, 55 and 53%, respectively (Figure 3). The detrimental impact of minor acid gases on the $CO_2$ adsorption capacity may be due to both physical and chemical adsorption mechanisms. In fact, several studies have demonstrated the adsorptive properties of acidic gases such as $SO_2$ and HCl onto activated carbons and amino-functionalized silica sorbents [35,43-47]. Physisorption processes of the acid gases over the surface of the material are mainly associated with high values of microporosity [43-46]. This assumption would explain the notable loss of $CO_2$ capture capacity of AC-1, which shows the highest microporous volume (Table 2). However, as it was already mentioned, other parameters such as the degree of surface functionalization of the sorbent and the presence of mercury in the flue gas need to be considered.

Chemisorption processes are due to reactions between either the nitrogen/oxygen groups on the surface of the activated carbons [44,45,47], or the amino groups in SBA-PEI and SBA-TEPA [19-21,48,49], and acidic gases present in the flue gas. The interaction between HCl with the C-O and C=O groups and between $SO_2$ with the basic active centers could contribute to the degradation of the carbonaceous adsorbents or the amines loaded and, therefore, decrease their $CO_2$ adsorption capacity. The $SO_2$-amine

interaction depends on the type of the amino group (primary, secondary or tertiary) [19,49,50] of the amino-functionalized adsorbents. As a matter of fact, the $CO_2$ capacity loss for SBA-TEPA is much higher than for SBA-PEI (Figure 3 (B)). This observation might be a consequence of the presence of a higher amount of secondary amines in the SBA-TEPA structure (60 %), in contrast to branched SBA-PEI (39 %). It has been reported before that secondary amines adsorb more $SO_2$ than primary and tertiary amines with comparable amine loading [49,50]. In other words, the strong reaction activity of $SO_2$ with TEPA [51] and the possible formation of sulphates and/or sulphites on the surface of the adsorbents may compete for the same adsorption sites as $CO_2$ [19-21,48,49], decreasing adsorbents adsorption capacity. Some authors have also demonstrated a higher HCl adsorption on sorbents treated with ammonia over untreated materials [52]. It makes then plausible to deduce that, even in presence of mercury, HCl in the gas stream could contribute to an increased loss of $CO_2$ adsorption capacity, since the $CO_2$ mass uptake registered in this study was lower than the obtained in a previous work [19] with the same adsorbents but under an atmosphere free of HCl.

The mercury retention capacity for the different sorbents was also calculated under the complete atmosphere (CA) (Table 4, Figure 5). In general, the aforementioned capacity is lower than the one obtained under a $N_2$+$CO_2$+Hg atmosphere. This fact should be taken into account mainly in the sorbents with high mercury retention capacity, i.e. AC-1. The effect of $SO_2$ on Hg capture by activated carbons has been widely studied [42,53,54]. The occurrence of $SO_2$ in the flue gas seems to be competing with mercury for the same binding sites, especially in those activated carbons with the highest micropore volume (AC-1).

### 3.5. Regeneration of sorbents.

The stability of adsorbent materials over consecutive adsorption-desorption cycles plays an important role in maximizing their lifetime which in turn affects the operating cost of the $CO_2$ capture process. Therefore, it is essential not only to evaluate the adsorption capacity of the sorbents but also to investigate the performance of the materials under cyclic conditions. Only those sorbents that performed best in the previously described adsorptions studies, AC-1 and SBA-PEI, were selected for the regeneration study. Eight adsorption-desorption cycles under the three different atmospheres were performed at room temperature for each sorbent. Under a binary mixture of 85%$N_2$ + 15%$CO_2$, the $CO_2$ capacity of activated carbons decreased from the first to the second adsorption cycle with no important changes throughout successive cycles. Regarding AC-1, this drop represented a loss of 12.4% in the $CO_2$ adsorption capacity from cycle 1 to 2 while the rate of capacity loss decreased 8.4% from the second to the eighth cycle. Mesostructured silica sorbents maintained almost the same adsorption capacity after 8 cycles.

It must be emphasized that when mercury was added to the $CO_2$+$N_2$ binary mixture, AC-1 underwent a gradual loss in its $CO_2$ adsorption capacity after the first cycle (29%) (Figure 6). This drop was especially dramatic (79% from cycle 1 to 2) in presence of the complete atmosphere, due to not only its high mercury retention capacity (Table 4) but also to the adsorptive properties of acidic gases onto the surface of this activated carbon. For SBA-PEI, although it suffered an important decrease of the $CO_2$ adsorption capacity, this loss remained almost invariable after the sorbent regeneration. This results point that the supported amine adsorbents (chemical adsorption), are reasonably stable to the flue gas pollutants, especially the sorbent SBA-PEI, during cycling adsorption operation at the conditions evaluated in this work.

## 4. Conclusions.

In general, the presence of mercury in the flue gas decreased the $CO_2$ mass uptake in the sorbents, suggesting a competition for the same active sites on the surface of the sorbents. This fact was particularly relevant in those sorbents with the highest mercury retention capacity.

The presence of acid gases ($SO_2$ and HCl) in flue gas composition also resulted in a notable decrease of the $CO_2$ adsorption capacity of the sorbents evaluated. This drop could be attributed to physisorption processes of these gases over the surface of activated carbons with high microporosity or might be consequence of the interactions between HCl/$SO_2$ and amines of functionalized sorbents, which are especially strong with secondary amines.

Although the presence of mercury and acid gases in the flue gas resulted in $CO_2$ capacity loss, aminosilica adsorbents based on poly(ethylenimine) (PEI), where occurred mainly a chemical adsorption, maintained a reasonable $CO_2$ capacity over a number of cycles, suggesting that they are stable to flue gas pollutants.

## Acknowledgments.

The financial support for this work was provided by the project CTQ2014-58110-R. The authors thank PCTI Asturias for awarding N. Fernández Miranda a pre-doctoral fellowship.

## References.

[1] S.Y. Lee, S.J. Park, A review on solid adsorbents for carbon dioxide capture, J. Ind. Eng. Chem. 23 (2015) 1–11.

[2] D.Y.C. Leung, G. Caramanna, M. M. Maroto-Valer, An overview of current status of carbon dioxide capture and storage technologies, Renew. Sustainable Energy Rev. 39 (2014) 426–443.

[3] D. Zhao, J. Feng, Q. Huo, N. Melosh, G.H. Fredrickson, B.F. Chmelka, G.D. Stucky, Triblock copolymer syntheses of mesoporous silica with periodic 50 to 300 Angstrom pores, Science 279 (1998) 548-552.

[4] A. Samanta, A.Zhao, K.H. George Partha, S. Sarkar, R. Gupta, Post combustion $CO_2$ capture using solid sorbents: a review, Ind. Eng. Chem. Res. 51 (2012) 1438-1463.

[5] J. Wang, L. Liang Huang, R. Yang, Z. Zhang, J. Wu, Y. Gao, Q. Wang, D. O'Hareb, Z.Z. Zhong, Recent advances in solid sorbents for $CO_2$ capture and new development trends, Energ. Environ. Sci. 7 (2014) 3478-3518.

[6] T.C. Drage, O. Kozynchenko, C. Pevida, M.G. Plaza, F. Rubiera, J.J. Pis, C.E. Snape, S. Tenninson, Evaluation of activated carbon adsorbents for $CO_2$ capture in gasification, Energy Procedia, 1 (2009) 599-605.

[7] A. Arenillas, K.M. Smith, T.C. Drage, C.E. Snape, $CO_2$ capture using some fly ash-derived carbon materials, Fuel 84 (2005) 2204.

[8] D.M. Ruthven, Principles of Adsorption and Adsorption Processes, Wiley-Interscience, New York, 1984.

[9] M. Caplow, Kinetics of carbamate formation and breakdown, J. Am. Chem Soc. 90 (1968) 6795-6803.

[10] P.V. Danckwerts, The reaction of $CO_2$ with ethanolamines, Chem. Eng. Sci. 34 (1976) 443-446.

[11] X. Xu, C.S. Song, B.G. Miller, A.W. Scaroni, Influence of moisture on $CO_2$ separation from gas mixture by nanoporous adsorbent based on polyethyleneimine-modified molecular sieve MCM-41, Ind. Eng. Chem. Res. 44 (2005) 8113-8119.

[12] X. Xu, C.S. Song, B.G. Miller, A.W. Scaroni, Adsorption separation of carbon dioxide from flue gas of natural gas-fired boiler by a novel nanoporous "molecular basket" adsorbent, Fuel Process. Technol. 86 (2005) 1457-1472.

[13] J. Mugge, H. Bosch, T. Reith, Gas adsorption kinetics in activated carbon, In. Adsorption Science and Technology: Proceedings of the Second Pacific Basin on Adsorption Science and Technology, Brisbane, Australia, May 14-18 (2000) 451-455.

[14] UNEP, Global Mercury Assessment 2013: Sources, Emissions, Releases and Environmental Transport, UNEP Chemicals Branch, Geneva, Switzerland (2013).

[15] M.L. Contreras Rodriguez, Study of trace metals behavior during coal and biomass cofiring in fluidized bed combustion, Thesis, Universidad Autónoma de Madrid, (2011) 465pp.

[16] K.C. Galbreath, C.J. Zygarlicke, Mercury transformations in coal combustion flue gas, Fuel Process. Technol. 65-66 (2000) 289-310.

[17] T.K. Gale, B.W. Lani, G.R. Offen, Mechanisms governing the fate of mercury in coal-fired power systems, Fuel Process. Technol. 89 (2008) 139-151.

[18] R. Sanz, G. Calleja, A. Arencibia, E.S. Sanz-Perez, Amino functionalized mesostructured SBA-15 silica for $CO_2$ capture: Exploring the relation between the adsorption capacity and the distribution of amino groups by TEM, Micropor. Mesopor. Mat. 158 (2012) 309-317.

[19] E. S. Sanz-Perez, M. Olivares-Marín, A. Arencibia, R. Sanz, G. Calleja, M.M. Maroto-Valer, $CO_2$ adsorption performance of amino-functionalized SBA-15 under post-combustion conditions, Int. J. Greenh. Gas Con. 17 (2013) 366-375.

[20] X. Xu, C. Song, J.M. Andrésen, B.G. Miller, A.W. Scaroni, Preparation and characterization of novel $CO_2$ molecular basket adsorbents based on polymer modified mesoporous molecular sieve MCM-41, Micropor. Mesopor. Mat. 62 (2003) 29.

[21] X. Xu, C. Song, R. Wincek, J.M. Andrésen, B.G. Miller, A.W. Scaroni, Separation of $CO_2$ from power plant flue gas using a novel $CO_2$ molecular basket adsorbent, Fuel Chemistry Division Preprints 48 (2003) 162.

[22] K.S.W. Sing, D.H. Everett, R.A.W. Haul, L. Moscou, R.A. Pierotti, J. Rouquerol, T. Siemieniewska, Reporting physisorption data for gas/solid systems with special reference to the determination of surface area and porosity, Pure Appl. Chem. 57 (1985) 603-619.

[23] A. Fuente-Cuesta, M. Diaz-Somoano, M.A. Lopez-Anton, M.R. Martinez-Tarazona, Oxidised mercury determination from combustion gases using an ionic exchanger, Fuel 122 (2014) 218−222.

[24] D. Cazorla-Amoros, J. Alcañiz-Monge, A. Linares-Solano, Characterization of activated carbon fibers by $CO_2$ adsorption, Langmuir 12 (1996) 2820-2824.

[25] E.S. Kikkinides, R.T. Yang, Concentration and recovery of $CO_2$ from flue gas by pressure swing adsorption, Ind. Eng. Chem. Res. 32 (1993) 2714-2720.

[26] B.K. Na, K.K. Koo, H.M. Wum, H. Lee, H.K Song, $CO_2$ recovery from flue gas by PSA process using activated carbons, Korean J. Chem. Eng. 18 (2001) 220-227.

[27] R.V. Siriwardane, M.S. Shen, E.P. Fisher, J.A. Poston, Adsorption of $CO_2$ on molecular sieves and activated carbon, Energy Fuels, 15 (2001) 279-284.

[28] M. Radosz, X. Hu, K. Krutkrarnelis, Y. Shen, Flue-gas carbon capture on carbonaceous sorbents: towards a low-cost multifunctional carbon filter for "green" energy producers, Ind. Eng. Chem. Res. 47 (2008) 3783-3794.

[29] A. Samanta, A. Zhao, G.K.H. Shimizu, P. Sarkar, R. Gupta, Post-combustion $CO_2$ capture using solid sorbents: a review, Ind. Eng. Chem. Res. 51 (2012) 1438-1463.

[30] H.M. Yoo, S.Y. Lee, S.J Park, Ordered nanoporous carbon for increasing $CO_2$ capture, J. Solid State Chem. 197 (2013) 361-365.

[31] N.P. Wichramaratne, M. Jaroniec, Importance of small micropores in $CO_2$ capture by phenolic resin-based activated carbon spheres, J. Mater. Chem. A. 1 (2013) 112-116.

[32] S.Y. Lee, S.J. Park, Determination of the optimal pore size for improved $CO_2$ adsorption in activated carbon fibers, J. Colloid Interface Sci. 389 (2013) 230-235

[33] M.B. Yue, L.B. Sun, Y. Cao, A. J. Wang, Y. Wang, Q. Yu, J.H. Zhu, Promoting the $CO_2$ adsorption in the amine-containing SBA-15 by hydroxyl group, Micropor. Mesopor. Mat. 114 (2008) 74-81.

[34] N. Fernández-Miranda, M.A. López-Anton, M. Díaz-Somoano, R.M. Martinez-Tarazona, Mercury oxidation in catalysts used for selective reduction on NOx (SCR) in oxy-fuel combustion, Chem. Eng. J. 285 (2016) 77-82.

[35] T.R. Carey, O.W. Hargrove, C.F. Richardson, Factors affecting mercury control in utility flue gas activated carbon, J. Air Waste Manage. Assoc. 48 (1998) 1166-1174.

[36] H. Yang, Z. Xu, M. Fan, A.E. Bland, R.R.. Judkins, Adsorbents for capturing mercury in coal-fired-boiler flue gas, J. Hazard. Mater. 146 (2007) 1-11.

[37] G. Skodras, Ir. Diamantopouloy, P. Natas, A. Palladas, G.P. Sakellaropoulos, Postcombustion measures for cleaner solid fuels combustion: activated carbons for toxic pollutants removal from flue gases, Energy Fuels 19 (2005) 2317-2327.

[38] G. Skodras, Ir. Diamantopoulou, A. Zabaniotou, G. Stavropoulos, G.P. Sakellaropoulos, Enhance mercury adsorption in activated carbons from biomass materials and waste tires, Fuel Proc. Techon. 88 (2007) 749-758.

[39] R. Yan, T.D. Liang, L. Tsen, P.Y. Wong, Bench-scale experimental evaluation of carbon performance on mercury vapor adsorption, Fuel 83 (2004) 2401-2409.

[40] Y.H. Li, C.W. Lee, B.K. Gullett, Importance of activated carbon´s oxygen surface functional groups on elemental mercury adsorption, Fuel 82 (2003) 451-457.

[41] J. Liu, M.A. Cheney, F. Wu, M. Li, Effects of chemical functional groups on elemental mercury adsorption on carbonaceous surfaces, J. Hazard. Mater. 186 (2011) 108-113.

[42] M.A. López-Antón, M. Rumayor, M. Diaz-Somoano, M.R. Martinez-Tarazona, Influence of a $CO_2$-enriched flue gas on mercury capture by activated carbons, Chem. Eng. J. 262 (2015) 1237-1343.

[43] F. Rodriguez-Reinoso, M. Molina-Sabio, M.A. Muñecas, Effect of microporosity and oxygen surface groups of activated carbon in the adsorption of molecules of different polarity, J. Phys. Chem. 96 (1992) 2707-2713.

[44] C. Moreno-Castilla, F. Marin-Carrasco, E. Hidalgo-Utrera, J. Rivera-Utrilla, Activated carbons as adsorbents of $SO_2$ in flowing air. Effect of their pore texture and surface basicity, Langmuir 9 (1993) 1378-1383.

[45] M. Molina-Sabio, M.A. Muñecas, F. Rodriguez-Reinoso, B. McEnaney, Adsorption of $CO_2$ and $SO_2$ on activated carbons with a wide range of micropore size distribution, Carbon 33 (1995) 1777-1782.

[46] Z. Wang, H. Liu, K. Zhou, P. Fu, H. Zeng, J. Qiu, Effect of surface oxygen/nitrogen groups on hydrogen chloride removal using modified viscose-based activated carbon fibers, RSC Adv. 5 (2015) 86005-86012.

[47] P. Davini, Adsorption and desorption of $SO_2$ on active carbon: The effect of surface basic groups, Carbon 28 (1990) 565-571.

[48] D. Chang, S.A. Bedell, L.H. Kirby, Method of simultaneous absorption of sulphur dioxide and nitric oxide from flue gas, U.S. Patent 5.433.934 (1995).

[49] F. Rezaei, C.W. Jones, Stability of supported amine adsorbents to $SO_2$ and NOx in postcombustion $CO_2$ capture 1. Single-Component Adsorption, Ind. Eng. Chem. Res. 52 (2013) 12192-12201.

[50] F. Rezaei, C.W. Jones, Stability of supported amine adsorbents to $SO_2$ and NOx in postcombustion $CO_2$ capture 2. Multicomponent adsorption, Ind. Eng. Chem. Res. 53 (2014) 12103-12110.

[51] Q. Liu, B. Xiong, J. Shi, M. Tao, Y. He, Y. Shi, Enhanced tolerance to flue gas contaminants on carbon dioxide capture using amine-functionalized multiwalled carbon nanotubes, Energy Fuels 28 (2014) 6494-6501.

[52] C.L. Mangun, K.R. Benak, J. Economy, K.L. Foster, Surface chemistry, pore sizes and adsorption properties of activated carbons fibers and precursors treated with ammonia, Carbon 39 (2001) 1809-1820.

[53] A.A. Presto, E.J. Granite, Impact of sulfur oxides on mercury capture by activated carbon, Environ. Sci. Technol. 41 (2007) 6579-6584.

[54] E.J. Granite, A.A. Presto, Comment on the role of $SO_2$ for elemental mercury removal from coal combustion flue gas by activated carbon, Energy Fuels 22 (2008) 3557-3558.

**Table 1**. Composition of the atmospheres evaluated.

| | $N_2$+$CO_2$ | $N_2$+$CO_2$+Hg | CA |
|---|---|---|---|
| $N_2$ (% v/v) | 85 | 85 | 79 |
| $CO_2$ (% v/v) | 15 | 15 | 15 |
| $O_2$ (% v/v) | ··· | ··· | 6 |
| $SO_2$ (ppm) | ··· | ··· | 50 |
| HCl (ppm) | ··· | ··· | 25 |
| Hg ($\mu g/m^3$) | ··· | 500 | 500 |

**Table 2**. Physical properties of $CO_2$ sorbents.

| | **Precursors** | **Surface area ($m^2 \cdot g^{-1}$)** | **Micropore volume $V_{DR}$ ($cm^3 \cdot g^{-1}$)** | **Micropore diameter $W_{DR}$ (nm)** | **Energy $E_{DR}$ ($kJ \cdot mol^{-1}$)** |
|---|---|---|---|---|---|
| AC-1 | coconut shell | 674 | 0.28 | 0.88 | 10.26 |
| AC-2 | anthracite coal | 416 | 0.17 | 0.85 | 10.70 |
| AC-3 | anthracite coal | 455 | 0.19 | 0.88 | 10.32 |

**Table 3**. Physical properties of amino-functionalized silica sorbents.

| | **Precursors** | **Surface area *BET* ($m^2 \cdot g^{-1}$)** | **Pore volume ($cm^3 \cdot g^{-1}$)** | **Pore diameter (nm)** | **% N** | **% amine (% w/w)** |
|---|---|---|---|---|---|---|
| SBA-PEI | silica | 153 | 0.27 | 5.8 | 5.8 | 30 |
| SBA-TEPA | silica | 220 | 0.45 | 9.0 | 8.8 | 30 |

**Table 4**. Mercury accumulated during eight experiments corresponding to eight cycles of $CO_2$ adsorption-desorption and $CO_2$ adsorption capacity under different gas compositions at room temperature and 1 bar of pressure.

| Adsorbents | Hg ($\mu g \cdot g^{-1}$) | | $CO_2$ (%) | | |
|---|---|---|---|---|---|
| | $N_2$+$CO_2$ | CA | $N_2$+$CO_2$ | $N_2$+$CO_2$+Hg | CA |
| AC-1 | 39.8 | 30.0 | 6.14 | 2.03 | 0.42 |
| AC-2 | 4.48 | 2.13 | 2.62 | 2.45 | 1.59 |
| AC-3 | 20.0 | 25.0 | 3.99 | 3.71 | 1.78 |
| SBA-PEI | 0.15 | 0.11 | 6.89 | 4.65 | 3.19 |

| | | | | | |
|---|---|---|---|---|---|
| SBA-TEPA | 0.07 | 0.04 | 5.55 | 5.52 | 0.41 |

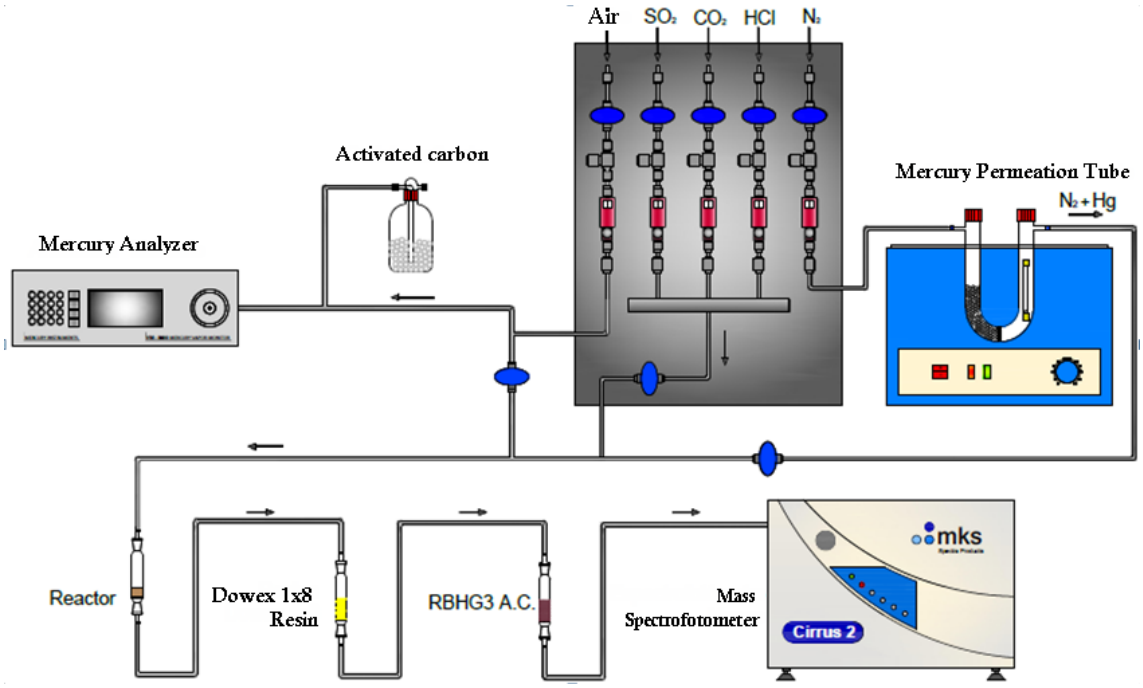


**Figure 1.** Laboratory-scale device employed in the assessment of the $CO_2$/Hg adsorption tests.

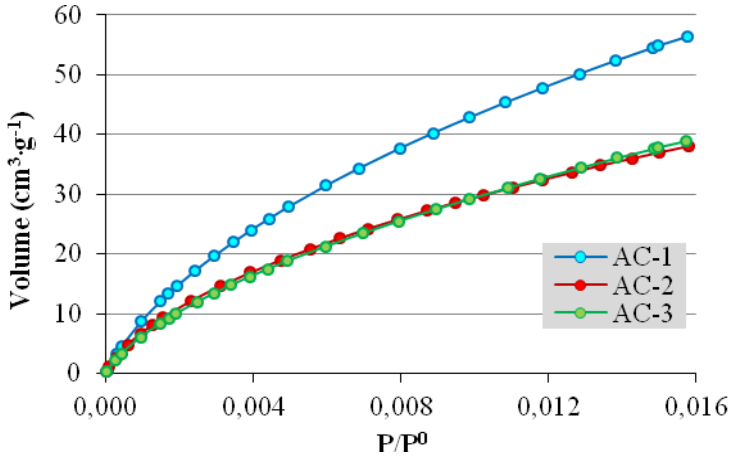

**Figure 2**. $CO_2$ adsorption isotherms of the activated carbon samples (at 25 ºC).

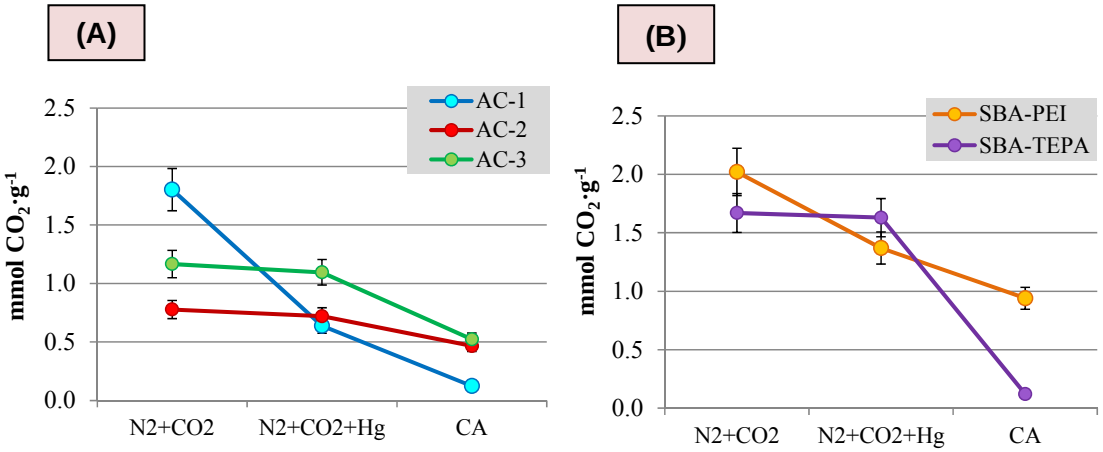


**Figure 3.** $CO_2$ adsorption capacity at 25 ºC and atmospheric pressure of (A) the activated carbons and (B) the amino-functionalized silica sorbents under different atmospheres.

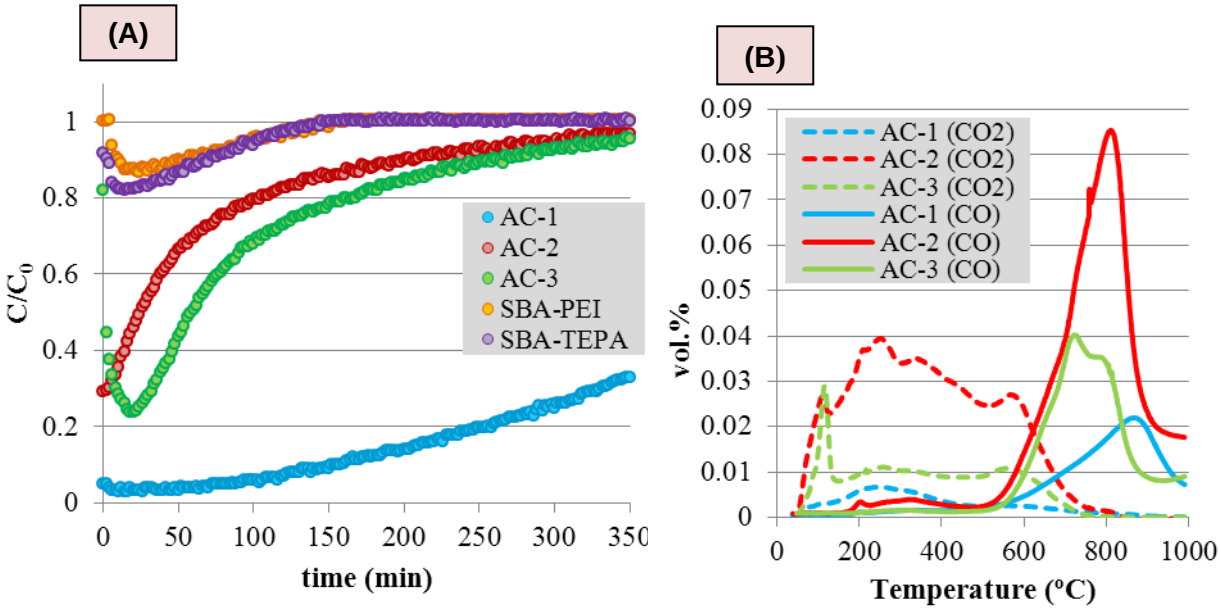


**Figure 4.** Mercury adsorption curves (A) at room temperature in an atmosphere with 85%$N_2$ + 15%$CO_2$ + [$Hg^0$] = 500 µg·$m^{-3}$ and TPD profiles (B) of CO and $CO_2$ evolution of the material employed.

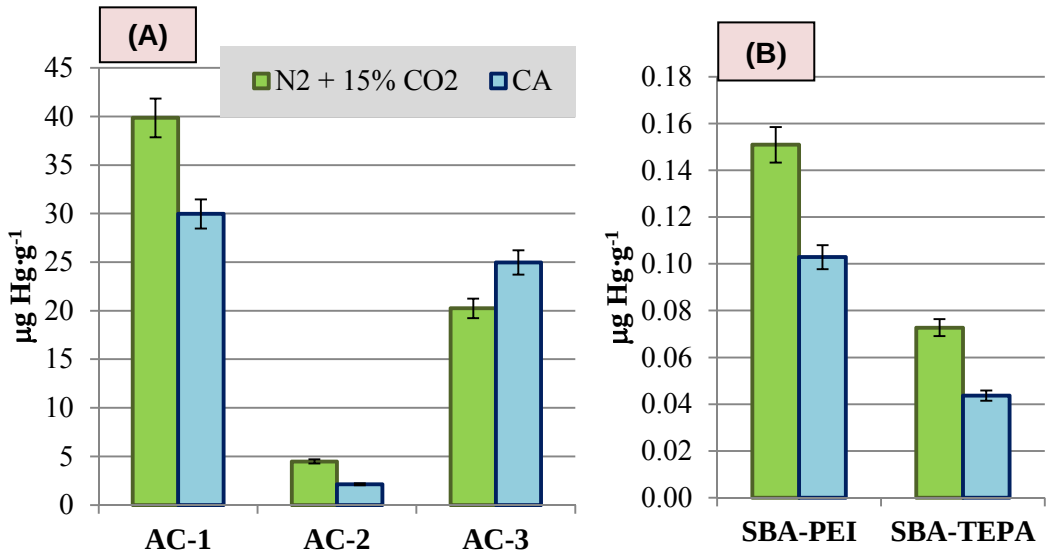


**Figure 5.** Mercury accumulated during eight experiments corresponding to eight cycles of $CO_2$ adsorption-desorption under different gas compositions for (A) the activated carbons and (B) the amino-functionalized silica sorbents.

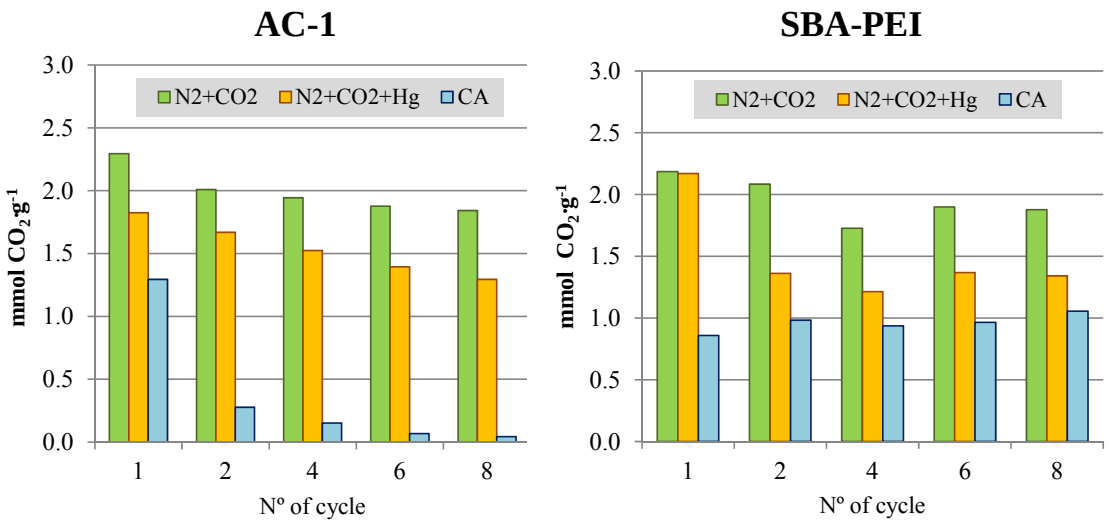

**Figure 6.** Mass uptake of AC-1 and SBA-PEI for $CO_2$ adsorption experiments in cycles 1, 2, 4, 6 and 8 under different gas compositions.